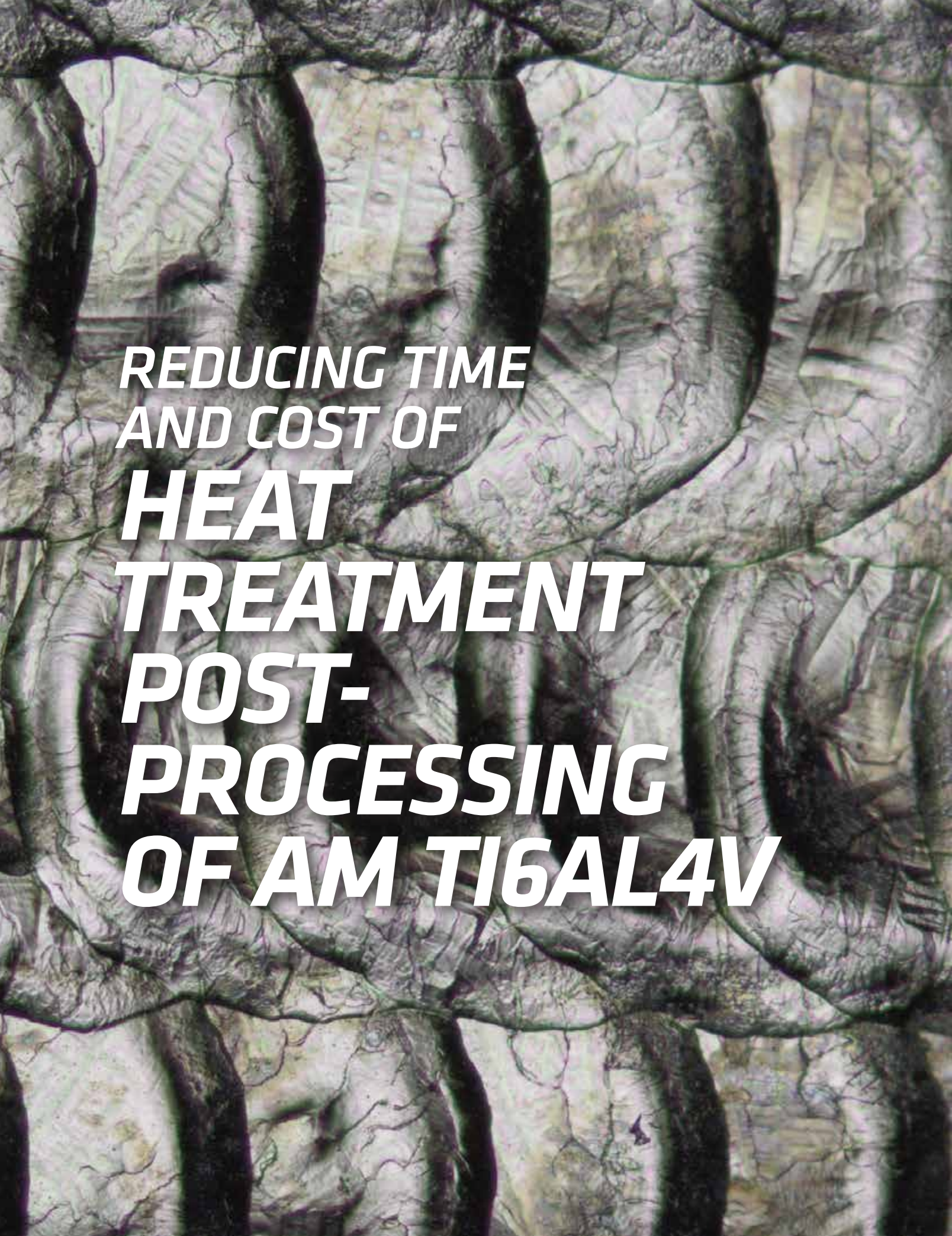

REDUCING TIME AND COST OF HEAT TREATMENT POST-PROCESSING OF AM TI6AL4V

An alternative vacuum heat-treatment cycle, considering all the technical aspects of additive manufacturing, can be used to save time and money.

By DEAN KOUPRIANOFF and WILLIE DU PREEZ

The unique microstructure of Ti6Al4V produced through laser powder bed fusion (LPBF) displays high-tensile strength with low elongation in the as-built state. To obtain desired material properties that comply with standards for Ti6Al4V products, further post-processing is needed. Conventional practice prescribes that the required tensile properties can be achieved with time-consuming post-processing heat treatment of LPBF parts, most of which use air or water quenching that causes surface modification, such as oxidation, when applied to Ti6Al4V. The aim of this work was to develop an alternative heat-treatment process that would retain the benefit of additive manufacturing (AM) but reduce the related processing time and cost, while still complying with the part property specifications. A new heat-treatment cycle was hypothesized and tailored, resulting from a critical analysis of current practice found in literature and practiced in the Centre for Rapid Prototyping and Manufacturing (CRPM) of the Central University of Technology, Free State, based on the need for a quick and cost-effective cycle. By comparing the obtained material properties and microstructure with those of other common heat treatments, the cycle was found to be faster, lasting only four hours in total, and the material properties were superior to those of existing cycles. A high yield stress of 987 MPa was obtained while retaining a good elongation of 16 percent.

1 INTRODUCTION

The additive manufacturing (AM) application market is growing considerably for medical and aerospace applications [1]. Titanium alloys such as Ti6Al4V are especially desired due to the established market, biocompatibility, and high specific strength. Ti6Al4V is an alpha (hcp) + beta (bcc) alloy, which, depending on the processing, can deliver Widmanstätten, equiaxed, and bimodal microstructures with various microstructural parameters, all of which affect the mechanical properties [2]. Martensite formation in Ti6Al4V is based on the formation of an alpha phase supersaturated with substitutional vanadium during rapid cooling. Martensite decomposition generally follows a path of depleting the supersaturated vanadium in the alpha phase through precipitation of the beta phase along the grain boundaries upon heating. The ultra-fine martensitic microstructures with columnar prior-beta grains are unique to laser AM processes and differ for each specific process and parameter set [3]. Therefore, considerable research continues to qualify AM parts made from Ti6Al4V for medical implants and aerospace components. How the AM processes influence the microstructure is an important factor being investigated. More specifically, for certifying AM, many topical standards, including post-processing, are lacking [4], [5], [6]. Aerospace requires good tensile and fatigue properties. Ensuring the material complies with these standards will allow acceptance and safe implementation in safety-critical applications such as aircraft structural components. Many different post-processing heat treatments have been investigated to obtain the desired properties. Not only should these meet the required standards but for implementation in industry, three important factors related to laser powder bed fusion (LPBF) must be considered: residual stress, the feasibility of removing surface contamination resulting from thermal post-processing, and time.

It is important to tailor the microstructure and resulting mechanical properties of LPBF Ti6Al4V parts for specific industrial applications. Conventional heat treatment of Ti6Al4V does not apply for LPBF Ti6Al4V because the microstructure of LPBF parts differs from that of forged and cast Ti6Al4V. One of the important differences is that as-built LPBF Ti6Al4V parts display a very fine martensitic microstructure. This results from the kinetics during LPBF of Ti6Al4V, which differ from conventional forming processes [7]. Due to rapid solidification, various effects arise — among these are the generation of martensitic microstructure, induction of residual stresses, and formation of non-equilibrium phases [8], [9], [10]. The typical as-built yield strength for Ti6Al4V is approximately 1,150 MPa with 6.5% elongation [11]. The Ti6Al4V(ELI) specification for powder bed fusion processes (ASTM F3001–14) specifies that the minimum tensile strength, yield strength (YS) and elongation values for the thermally treated condition are 825 MPa, 760 MPa, and 8%, respectively, for both the horizontal- and vertical-build directions [12]. When comparing the as-built (AB) values of the mechanical properties reported by the authors mentioned above to the ASTM F3001–14 values, the AB exceeds the strength requirement significantly but does not meet the ductility requirement.

As-built LPBF Ti6Al4V parts usually consist of columnar prior-beta grains filled with extremely fine acicular α' martensite. The fine α' martensite obtained during LPBF differs from conventional α' martensite in the sense that the spacing is tight, with many dislocations and twins obstructing dislocation movement and therefore reducing ductility. Columnar prior-beta grain boundaries favor intergranular failure, which decreases ductility along with the negative effects of mechanical anisotropy and limited fatigue life. The cooling rate strongly influences the prior-beta grain size and the morphology of the α phase [13], [14].

Stress relieving to avoid distortion is a critical part of the LPBF process. Residual stress and microstructure greatly influence the fatigue properties and crack growth of titanium alloys. Van Zyl et al. [15] measured residual stress near the top surface of LPBF Ti6Al4V as-built samples attached to the substrate. Residual stresses were tensile and in the range of 200–800 MPa. A stress of 800 MPa is only 30 MPa below the typical YS of annealed Ti6Al4V(ELI). Distortion can occur and cracks can initiate when removing the component from the substrate on which it was produced without prior stress-relieving heat treatment.

Therefore, stress relieving should be applied before removing the parts from the substrate. The standards AMS 2801 and SAE H81200 provide guidance on stress relief. Ter Haar and Becker (2020) found that, for stress-relieving temperatures above 560°C, 90% of the residual stress in LPBF parts was relieved and proposed a higher tempera-

ture of 650°C to give the best ductility. These findings are similar to those found for conventional Ti6Al4V stress-relieving temperatures given by Donachie (2000), who proposed that titanium stress relieving be done at temperatures between 480°C and 650°C for a time of one to four hours, resulting in more than 70% of the residual stress being relieved in the first hour. Ter Haar and Becker [16] also showed these stress-relieving temperatures (427-610°C) with long holding times could lead to the decomposition of martensite, but this resulted in embrittlement of the material due to fine β phase precipitates formed at α/α' grain boundaries.

The temperature at which SR occurs is not as critical as ensuring uniform temperature distribution upon cooling, especially from 480°C to 351°C. Stress relieving can be omitted if high-temperature annealing is carried out [2], [17].

To modify the LPBF microstructure, high-temperature annealing is employed. A well-known work by Vrancken et al. [7], in which many different heat treatments were investigated, found that no significant grain growth occurred for temperatures well below the beta transus. The fine α and β grain interfaces were found to limit grain growth. Only at 850°C did noticeable grain growth effects start to arise. When cooling from 850°C, because of the large fraction of α phase present, no significant change in microstructure was seen with a change in cooling rate. Contrary to conventional Ti6Al4V manufacturing methods, for which an increase in heat-treating temperature decreases the elongation with an increase in YS [2], with LPBF, the elongation values increase with an increase in annealing temperature at the expense of YS. Similarly, time spent below the beta transus had no significant effect on the grain growth, or, rather, no large grains were obtained, and the laminar structure remained. Even after considerable time, the laths were still relatively small, although they might have become less elongated [18], [19].

For LPBF, Yadroitsev et al. [20] showed that a globular microstructure could be obtained at higher temperatures and holding time. In their work, they obtained a globular microstructure by heating to 50°C below the beta transus, followed by a water quench. Ter Haar and Becker [21] suggested the optimal heat treatment for LPBF was a duplex anneal consisting of 910°C for eight hours, followed by a water quench and thereafter 750°C for four hours, followed by furnace cooling. Interestingly, they were able to produce a bi-modal microstructure with ultimate tensile stress (UTS) and elongation above 900 MPa and 15%, respectively. However, these two above-mentioned heat treatments are not feasible solutions for parts that cannot be machined or descaled because they also increase the post-processing time.

Some more recent approaches were from Sabban et al. [22], who obtained a globularized microstructure by cycling at between 975°C and 875°C with slow cooling between the cycles. Another team [23] was able to produce samples with quasi-equiaxed microstructures by using rapid heat treatment above the beta transus. Here, the refinement of prior-beta grain boundaries was reported for the first time.

Name	Ramp rate (°C/h)	Soak temp (°C)	Soak time (h)	Cooling rate (°C/h)
650-SR	200	650	3	Furnace
850-ANN	200	850	2	Furnace
895-ANN	200	895	2	Furnace
940-ANN	200	940	2	Furnace
650-SR&940-ANN	200	650, 940	3,2	Furnace
940-ANNGQ	200	940		
New-cycle	Described below		2	Gas quench

Table 1: Ti6Al4V heat treatment cycle times and temperatures.

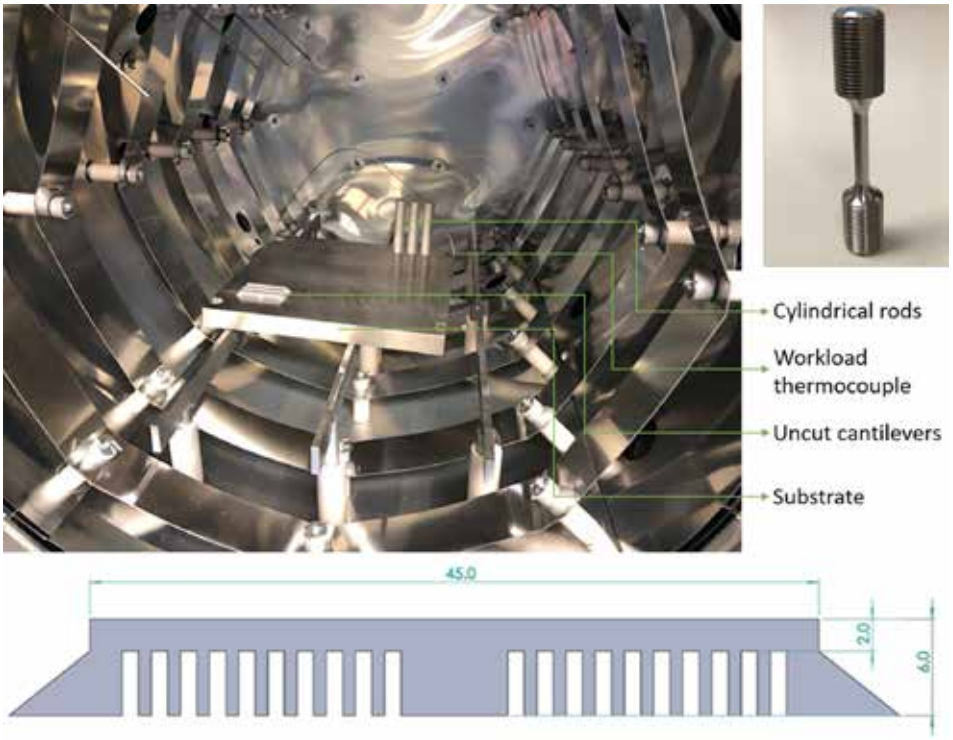

Figure 1: Ti6Al4V substrate with unmachined tensile rods and cantilevers inside the vacuum chamber. A typical machined tensile specimen is shown at the top right, and the cantilever specimen dimensions are at the bottom.

	Al	V	Fe	O	C	N	H
ASTM F 3001–14	5.5–6.5	3.5–4.5	<0.25	<0.13	<0.08	<0.05	<0.012
Current work	6.47	4.12	0.19	0.09	0.01	0.01	0.002

Table 2: Ti6Al4V(ELI) chemical composition and ASTM F 3001–14 requirements.

Baker et al. [24] proposed to the LPBF community that terminology that accurately describes the heat treatment history was needed. The term "high-temperature anneal" was proposed for fully lamellar microstructure. This need for new nomenclature confirmed the development and growth in the field of LPBF post-processing.

To avoid oxygen pick-up, heat treatments can be done in a vacuum. The heat-treatment standard for Ti6Al4V LPBF (ASTM F3301–18a, 4: "Thermal Post-Processing Requirements") specifies that heat treatments should be carried out according to the conventional standard: AMS 2801 "Heat treatment of Titanium Alloy Parts" [25]. In AMS 2801, it is specified that (Notes: 8.5) to avoid surface contamination, parts should not be exposed to air above 204°C. In addition, AMS 2801 requires descaling for parts heated above 538°C in an environment other than an inert atmosphere or vacuum. Consequently, due to the

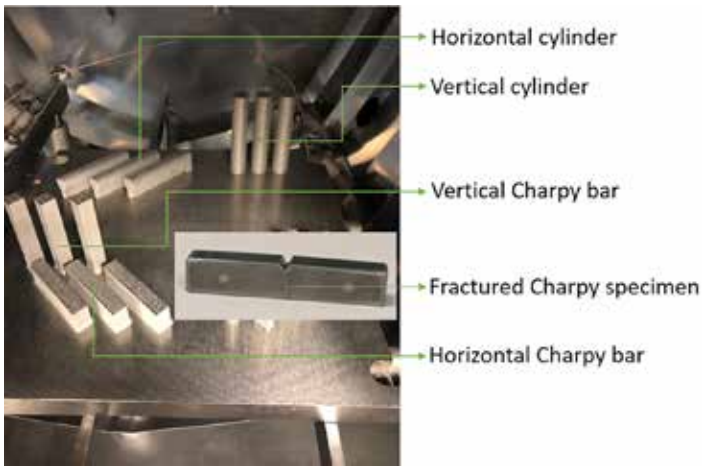

Figure 2: Charpy impact test specimen bars with a typical fractured specimen, as well as tensile test specimen cylinders on the substrate in the furnace chamber.

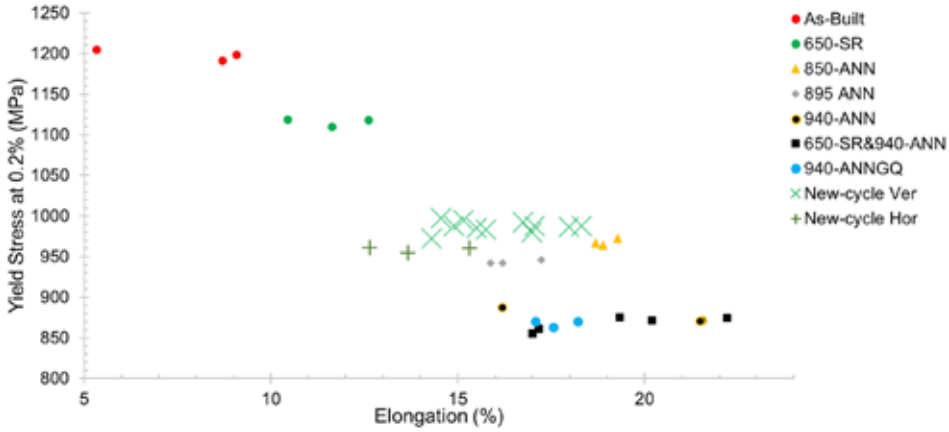

Figure 3: Yield stress vs % elongation for each cycle.

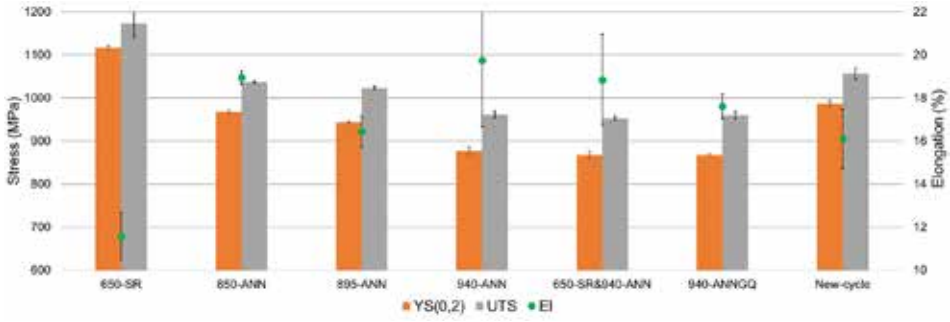

Figure 4: Engineering tensile properties of different heat treatments (stress on primary axis and elongation on secondary axis).

nature of LPBF, which has the advantage of directly delivering the net shape of a final part with complex geometry, conventional removal of surface oxides is normally not a feasible solution. Therefore, many of the suggested post-processes found in literature are not practical solutions for industries such as aerospace. While AMS 2801 specifies that stress relieving (SR) should consist of soaking at 593°C for two hours and annealing at 704°C for two hours, both occur above the temperature where descaling is required in the same standard. This implies that for LPBF of Ti6Al4V, only inert or vacuum atmospheres are suitable. Accordingly, AMS 2801 addresses this point by specifying that parts with net dimensions shall not be heated above 538°C in air or non-inert atmosphere furnaces unless coated with a protective coating, which is not always feasible with LPBF.

From the preceding discussion, vacuum heat treatment of titanium alloys is evidently the best solution because it has the benefits of not only removing contaminants from the atmosphere but also dissociating surface oxides. The use of vacuum heat treatment is also highly recommended by EOS to avoid the formation of alpha case on the surface of the parts [26].

Among the authors, the most common heat treatment that delivers good YS and elongation values (ASTM F3001–14: minimum of 825 MPa and 8%, respectively) seems to be a single-cycle heat treatment at 850-950°C followed by furnace cooling [7], [26], [27], [28], [29].

Despite their general acceptance, these thermal treatment cycles are still time-consuming and dependent on ramping rates, holding time/temperature and the cooling method used. Changes in these parameters result in different material properties; therefore, considerable care must be taken when altering these cycles. Typically, these heat-treatment cycles take more than nine hours to complete, implying that at least one day or night is needed for the parts to be thermally processed.

Therefore, the current study was undertaken to address the need for an alternative heat-treatment cycle that would reduce heat-treatment time and cost for the Centre for Rapid Prototyping and Manufacturing (CRPM) clients while still achieving the required properties. Assuming that the β grain growth is dependent on diffusion through its own grain boundary and that no considerable diffusion takes place below 750°C, a short time above this temperature is needed for the supersaturated elements to travel the length of the minor axis required for martensite to decompose into lamellar $\alpha + \beta$. This will retain the fine microstructure but lead to increased ductility. Yang et al. [14] were the first to show the development of the hierarchical structure of LPBF α' martensite (primary, secondary, ternary and quartic) caused by the thermal history. The hierarchical structure of acicular α' grains has an aspect ratio of between 10 and 20, with the minor axis of the primary α' and quartic α' being ~1-3 µm and 10-20 nm, respectively [14], [21]. The thinnest α martensite (quartic α') is smaller than 20 nm; thus, a very short diffusion path is present for the supersaturated atoms to travel within the grain and form the β phase on its grain boundary. Ti6Al4V has no significant diffusion below 750°C, but at 940°C the diffusion rate is approximately 0.07 µm^2/s and 0.05 µm^2/s for aluminum and vanadium in β titanium, respectively [30]. Even when considering the worst case, for large primary α' of 1 µm width and assuming only bulk diffusion of vanadium, the atoms at the grain center need to travel half the minor axis (0.5 µm). This equates to a rough estimate of ~10 s to traverse this distance. It shows the desired fine lamellar $\alpha + \beta$ morphology can be obtained in a very short time.

This rough calculation is based on bulk diffusion rates and does not consider factors such as the transient non-equilibrium chemical composition, as the supersaturated bulk initially rearranges atoms to precipitate in seed phases. At 882°C, the solubility of vanadium in α-Ti is zero; therefore, rapid rearrangement of atoms and β precipitation on the grain boundaries can be expected. Fine microstructural features like vacancies, high dislocation, and twin density will sig-

nificantly increase the diffusion rate due to grain boundary diffusion. Although the diffusion calculation is a simplified analysis, it shows that even for the slower bulk diffusion mechanism, only short times are needed at this temperature for the transformation, and it can be expected that the actual decomposition will be much faster. These short times reduce grain growth, leading to desirable fine microstructures as it increases material properties and can be particularly beneficial for fatigue and fracture mechanics. Additionally, since the sections of AM parts are generally smaller than industrial Ti6Al4V sections, there is no need for temperature soaking to ensure temperature uniformity. Therefore, the authors propose the use of a very short thermal treatment that would not only save time and money for the clients of the CRPM but would produce exceptional microstructural and material properties. This study compared these properties to those obtained through some of the most common post-heat treatments implemented in the AM industry.

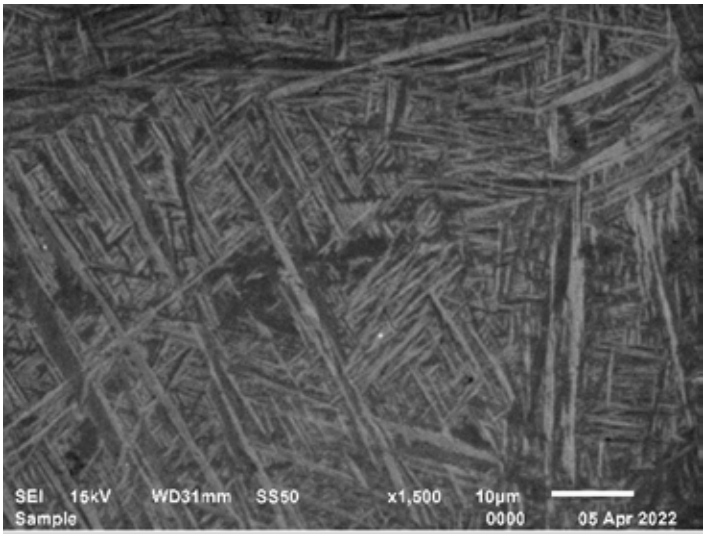

Figure 5: SEM micrograph of a cross-section of an as-built specimen in the XY plane.

2 METHODOLOGY

To compare the hypothesized cycle with conventional annealing (ANN) cycles found in literature, the cycles shown in Table 1 were investigated. Table 1 shows the heating parameters for each investigated cycle, hereafter referred to as 650-SR, 850-ANN, 895-ANN, 940-ANN, 650-SR&940-ANN, 940-ANNGQ and New-cycle, respectively.

The New-cycle consisted of ramping to 600°C at 300 °C/h, then ramping to 940°C at 637.5°C/h, followed by immediately ramping down to 600°C at 637.5°C/h. This was followed by a furnace cool to 400°C. On reaching 400°C, argon gas was introduced and kept stationary until 300°C was reached, whereafter, the quick-cooling fan was turned on for cooling to room temperature.

The vacuum heat treatment was carried out using a T-M Vacuum Products Inc. SS12/24–13MDX vacuum furnace operated consistently at vacuum levels < 0.01 µm Hg, which exceeds the recommended (AMS 2801B) level of 0.1 µm Hg. The vacuum chamber with the platform on which the Ti6Al4V(ELI) test specimens were loaded is shown in Figure 1.

Test specimens of Ti6Al4V(ELI) were produced in an EOS M290 DMLS machine at standard EOS Ti6Al4V process parameters laser power: 280 W, scanning speed: 1,300 m/s, hatch distance: 150 µm and layer thickness: 40 µm from powder with the chemical composition shown in Table 2. The equivalent diameters (by volume) of the powder particles were d10=31 µm, d50=49 µm and d90=75 µm.

For each of the above-mentioned cycles, three cantilever specimens (dimensions shown in the diagram in Figure 1) and three vertical test specimen rods (aligned with the Z-axis of the machine) were manufactured and then heat treated. After each cycle, the T-shaped cantilevers were cut from the baseplate and the deformation was measured to compare the effectiveness of stress relief for each cycle. This measurement indicated the magnitude of residual stress in the material after removal: the cantilever deflection is caused by the stress, which can deform the material after cutting the anchor points from the substrate. The amount of strain was shown to be directly proportional to the residual stress [31], [32], [33]. The cylindrical rods

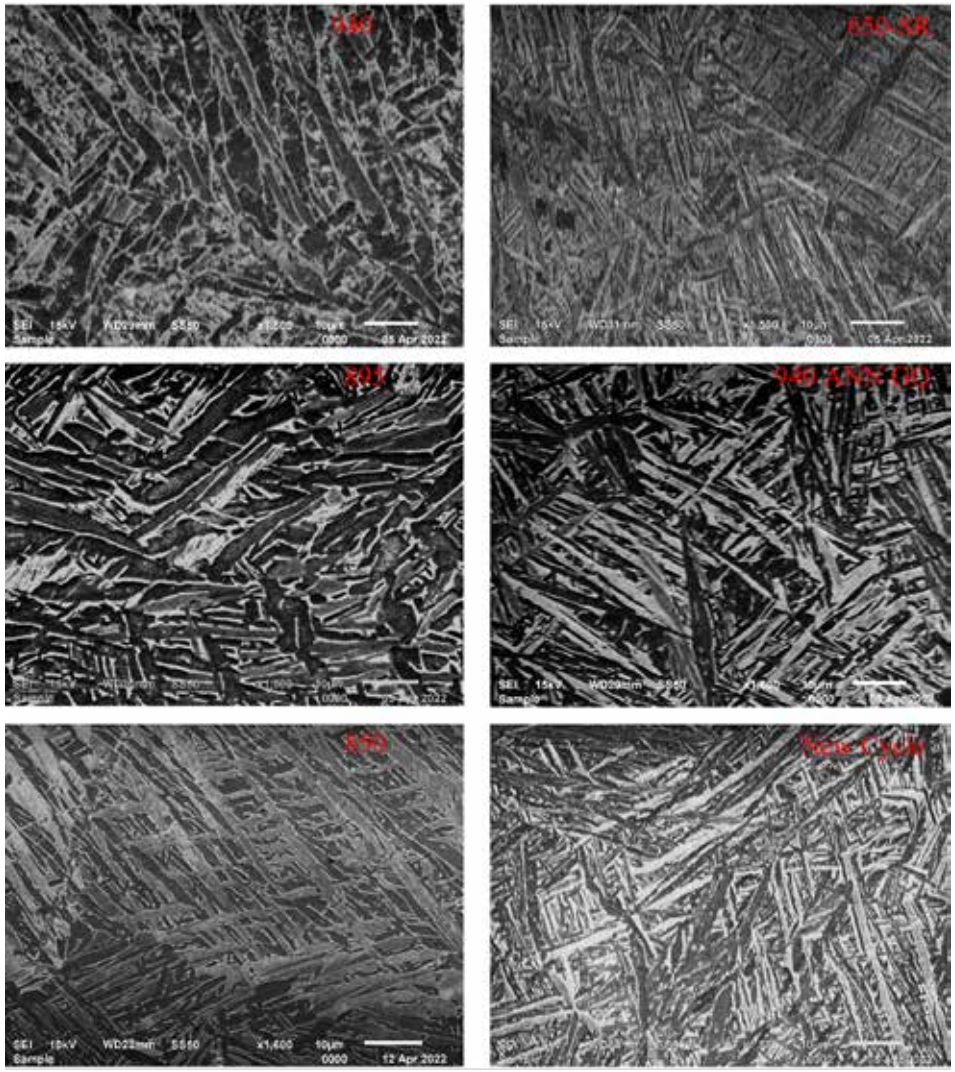

Figure 6: SEM micrographs of horizontal cross-sections (X-Y plane) showing the microstructures resulting from the corresponding heat treatment cycles.

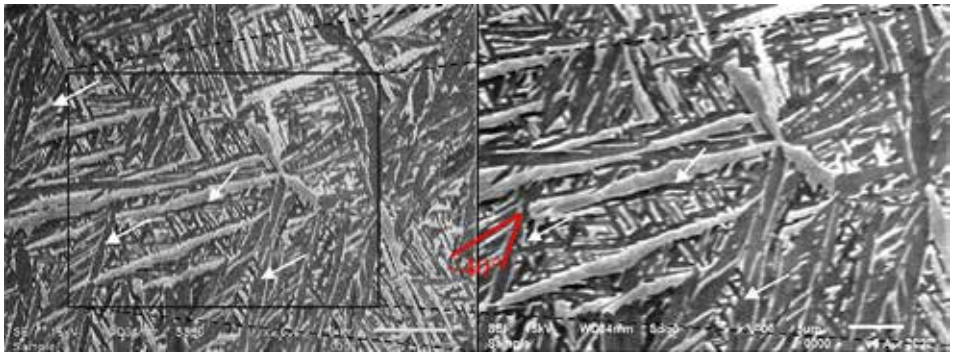

Figure 7: SEM micrographs of New-cycle showing alpha twin fragmentation indicated by arrows (left) and higher magnification of the square region (right).

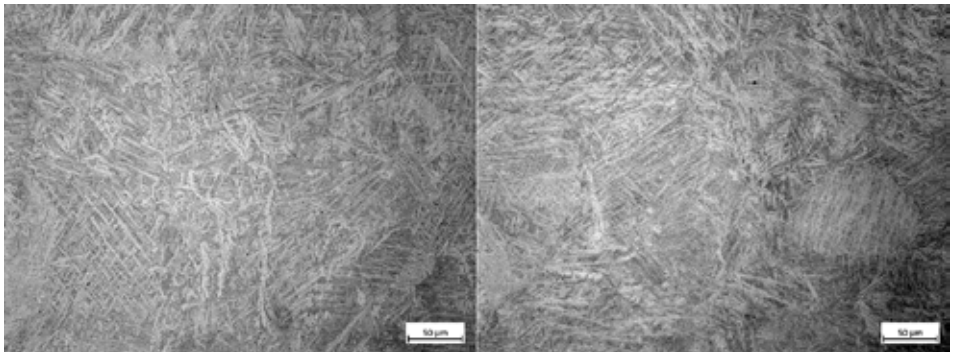

Figure 8: OM micrographs of 850-ANN (left) and New-cycle (right).

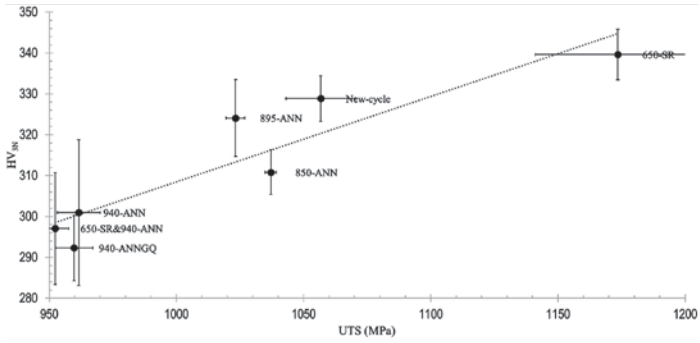

Figure 9: Microhardness vs UTS in the X-Y plane of the different cycles.

were machined according to ASTM E8 to produce tensile specimens with a gauge length of 16 mm. For microstructural analysis, the threaded ends of the tensile specimens were cut, polished, and etched with Kroll's reagent. A JEOL JSM-7800 F was used for scanning electron microscopy (SEM) and backscattered electron (BSE) imaging of the microstructure and fracture surfaces. The grain width of the lathes in the microstructures was measured with ImageJ software. To compare the impact of microstructural features of the different cycles, Vickers microhardness measurements were done at 3 N for 10 s on representative specimens from each type of heat treatment cycle.

Charpy impact testing was also done for the New-cycle, along with more tensile tests, resulting in 12 vertical tensile specimens from three different build orientations and treatments. Both the Charpy impact and tensile testing were performed on test specimens orientated in the vertical and horizontal building directions. The impact specimens were 100 × 10×10 mm with machined v-notches (see Figure 2). The 650-SR&940-ANN data was also obtained from five specimens, implying that the tensile properties and standard deviation data for the New-cycle and 650-SR&940-ANN were statistically more reliable.

3 RESULTS

None of the cantilevers used in the different heat-treatment cycles showed any deflection, confirming that all the cycles sufficiently relieved residual stresses. Figure 3 shows the yield stress versus the % elongation for each cycle.

Figure 3 shows the New-cycle performed well with 16.1% elongation and the highest yield stress of all the HTA specimens. For the 650-SR&940-ANN specimens, the additional stress-relieving cycle seemed to have no impact on the final material properties, which were very similar to those of the single 940-ANNGQ. This is shown more clearly in Figure 4, with the property values and standard deviations being similar for 940-ANN and 650-SR&940-ANN.

For the different HTA cycles, both the YS and UTS decrease with an increase in temperature. A significant increase in elongation is seen in the temperature range of 895-940°C, while a drop in elongation is seen between 850°C and 895°C, which has the same temperature range. This will be discussed in more detail later. The elongation of the 650-SR is the lowest because the alloy still has a martensitic microstructure (see Figure 5, Figure 6). On the other hand, the 650-SR specimens have the highest UTS, being 140 MPa above that of the 850-ANN specimens. For the 940-ANNGQ, the gas quench from the high temperature seemed to have had no impact on the strength when compared to furnace cooling from the same temperature. However, the 940-ANNGQ specimens did have slightly lower average elongation than the 940-ANN specimens.

Figure 5 shows the well-known, as-built fine martensite structure obtained by the LPBF process.

The corresponding microstructures of the other heat-treatment cycles can be seen in Figure 6. The AB and 650-SR microstructures are similar (Figure 5, Figure 6) in the sense that the fine needle-like microstructure is retained.

For the 940-ANNGQ cycle, the gas quench reintroduced high cooling rates, and its microstructure in Figure 6 shows that the 940°C anneal, followed by the higher cooling rate (gas quench), compared to the 940-ANN with furnace cool, did exhibit the same size of laths, but with sharper needle-like martensite shape.

For the New-cycle, some hierarchical α' substructures were still present, as shown in Figure 7. Here the smaller laths are clearly orientated to the larger ones indicating that the shape of the starting grain structure has been retained.

Figure 8 shows optical microscopy (OM) micrographs of cross-sections of the 850-ANN and the New-cycle specimens, which both display a fine $\alpha + \beta$ microstructure, although the 850-ANN is coarser due to the longer annealing time, which allowed the finer laths to be dissolved into adjacent grains (also compare the SEM images of 850-ANN and New-cycle in Figure 6). This New-cycle microstructure correlates with the EOS Titanium Ti64 Grade 23 material data sheet, which specifies that for a heat treatment of "120 min (±30 min) at 800°C (±10°C) measured from the part in vacuum (1.3×10^{-3} –1.3×10^{-5} mbar) followed by cooling under vacuum" the microstructure will consist of "fine alpha + beta ($\alpha+\beta$) phase" [26].

Heat treatment, which resulted in martensite decomposition into a fine alpha +beta microstructure, was between 800°C and 850°C. This is consistent with other findings [34], [35], [36]. It confirms that the fine microstructure obtained during the New-cycle was similar, although finer, than that of the other studies that used heat treatments between 800°C and 850°C. The finer $\alpha+\beta$ structure of the New-cycle promoted grain boundary strengthening and, hence, led to a higher yield stress than that of the 850-ANN. This was confirmed by the increased microhardness shown in Figure 9. The mean widths of the α laths in the microstructures obtained with the different heat treatments are given in Table 3.

The LPBF microstructure of Ti6Al4V(ELI) seemed to follow a Hall-Petch relationship in the sense that the fine martensitic grain structures showed the highest UTS, and as the size of the grains increased (as seen in Figure 6), the UTS and hardness decreased.

The microhardness trend seen in Figure 9 is similar to that reported by Malka-Markovitz et al. (2016), who reported that the hardness decreased as the martensite decomposed to α between the temperatures of 650°C (SR) and 850°C, but then from 850°C upward, the hardness increased as the α evolved into a bi-phasic $\alpha+\beta$ microstructure. Subsequently, a drop in hardness follows again with an increase in temperature as observed between 895°C and 940°C, which is due to the fine $\alpha+\beta$ microstructure that coarsened, resulting in a drop in hardness.

BSE images of the cross-sections of the specimens that have undergone the three annealing temperatures and the New-cycle are shown in Figure 10. A clear difference can be seen in the width and length of the laths resulting from the different cycles. The 940-ANN developed very long laths, with one long one clearly visible in the middle of the micrograph.

The microstructure in the XZ plane retains the columnar prior-beta grain morphology after the New-cycle heat treatment, as shown in Figure 11. The measured microhardness values were constant across the cross-section of the threaded section of a tensile specimen, as shown in Figure 11.

The New-cycle specimens had good impact toughness, as shown in Table 4. The lower impact toughness in the horizontal direction can be attributed to the directionality of the prior-beta columns leading to preferential crack propagation. It should be noted that, although the horizontal property values were lower than the vertical values for both the tensile and impact toughness, they exceeded the requirements of the Aerospace Specification Material for annealed Ti6Al4V(ELI) [37].

Fracture surfaces for both the vertical and horizontal impact specimens were the same. The fracture surfaces were flat and very smooth, with shear lips, as shown in Figure 12.

Similar to the grains' size reduction seen in the micrographs between the 940-ANN, 850-ANN and the New-cycle, the fractography of the tensile specimens showed the dimple sizes decreasing with temperature, as depicted in Figure 12. All specimens fractured in a ductile mode, and the fracture surface of the New-cycle showed the smallest dimples with a very uniform topography.

		850-ANN	895-ANN	940-ANN	New-Cycle
A lath width (µm)	mean	1.4	1.2	2.5	0.5
	stdev	0.6	0.5	0.8	0.3

Table 3: Width of alpha laths for 940-ANN, 895-ANN, 850-ANN and New-cycle.

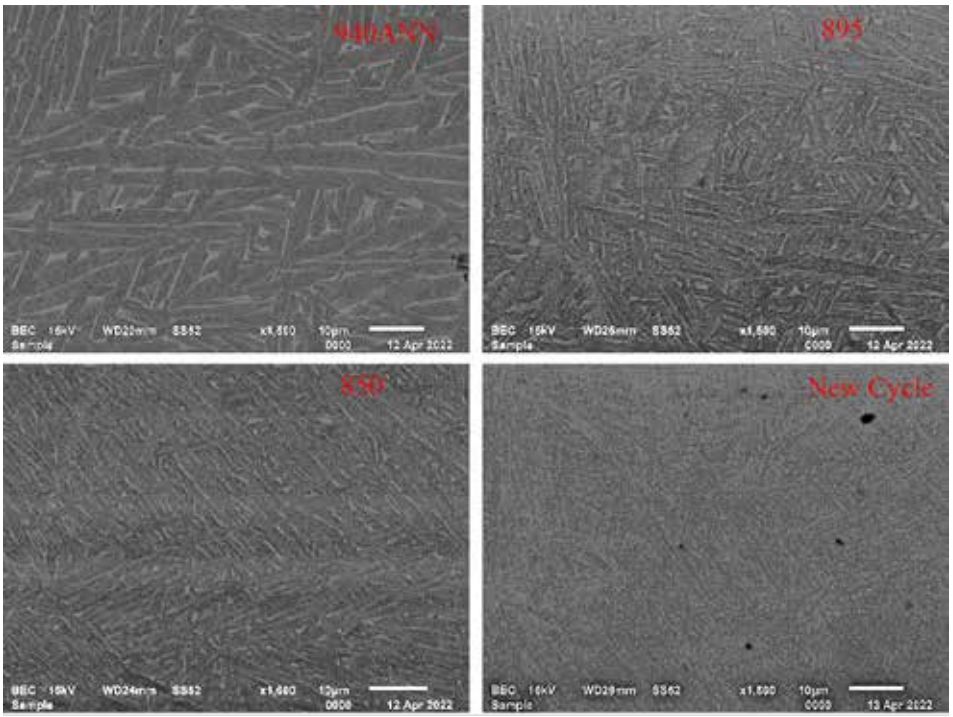

Figure 10: X-Y plane BSE images of 940-ANN, 895-ANN, 850-ANN and New-cycle (alpha = dark grey; beta = white).

Figure 11: Vertical (XZ plane) cross-section and microhardness across the threaded section of a New-cycle tensile specimen.

	Horizontal	Vertical
		
Impact toughness (J)	26.0 ± 2.0	33.3 ± 2.3

Table 4: V-notch impact toughness at 22°C of a specimen submitted to the New-cycle heat treatment.

4 DISCUSSION

4.1 Material properties

For the New-cycle, the vertically orientated specimens performed slightly better than the horizontally orientated ones, which had lower

elongation. This anisotropic nature of the tensile properties agrees with other findings [26], [35], [38], [39].

The vertical tensile properties reported by EOS for HTA at 800 for two hours are 980 MPa, 1050 MPa and 15% for $YS_{0.2}$, UTS, and elongation, respectively [26]. When considering the tensile results of the different heat treatments in Figure 4, the tensile properties resulting from New-cycle compare or exceed those reported by EOS and others [7], [21], [23], [26]. The 850-ANN shows an even higher elongation value with a slightly lower yield point, as shown in Figure 4. In general, all cycles showed good elongation, with the AB being 7.7%; an attributing factor can be the short interlayer time. All specimens were not built on one substrate but over multiple prints, i.e. for each different heat treatment, only three vertical rods were manufactured on the substrate. This results in a very short interlayer time, which has been shown to increase elongation due to coarsening of the α laths [40].

Ter Haar and Becker [21] showed that α-grain fragmentation during high-temperature annealing formed at twinning locations. During the New-cycle, fragmentation of α at twins occurred (see Figure 7), which, considering that the New-cycle was only kept at high temperatures for a brief time, confirmed that the fragmentation occurred rapidly at high temperatures. Some of the smaller ternary and quartic α had dissolved into the larger primary and secondary α grains. These laths, when compared to the AB microstructure shown in Figure 5, are larger and not as needle-like.

The grain structure of the New-cycle is considerably finer (submicron) compared to the other cycles and shows compositional contrast (Figure 10), verifying that the short holding time is sufficient for the supersaturated α' to decompose into a fine α+β phase. This agrees with Cao et al. [19], who showed that above 900°C, a time shorter than 0.5 h was needed to decompose the martensite. The alpha lath widths for 850-ANN and 895-ANN are very similar, explaining the similarities in tensile stresses (Figure 4), but the 895-ANN has reduced elongation as noted in the increase of hardness (Figure 9) when α evolved into a bi-phasic α+β microstructure [36]. Figure 11 shows good microstructural uniformity in the thick 12.5 mm sections. Although it is challenging to successfully build LPBF parts with large cross-sections due to residual stress, it was decided to simulate the New-cycle heat-treatment process to calculate the maximum temperature

difference for a 100 mm cube on the substrate. In a SolidWorks 2020 thermal study, the temperature vs. time profile was simulated while assuming that, for the vacuum heat treatment, the surface of the part was equal to the temperature measured by the thermocouples, and no conduction or convection occurred. For a simplified 100 mm cube, it was found that the maximum temperature difference would be ~40°C lower at the core, i.e. a maximum temperature of 900°C. However, this was not a concern, bearing in mind that the lower temperature anneals (895-ANN and 850-ANN) and 650-SR do give good tensile properties. It was noted that the microhardness measured on the cross-sections in the XZ plane was ~10 HV lower than that obtained in the XY plane. The New-cycle XY microhardness (329 HV) was below those of AB and 650-SR specimens of 352 HV and 340 HV, respectively, indicating that microstructural changes had occurred.

The New-cycle showed good impact toughness, with the values of the vertical specimens being considerably higher than other LPBF work in heat-treated conditions [41], [42], [43], [44]. This is an exciting finding and an area for further research, which might hold promising benefits for fatigue and fracture toughness.

Yonemura et al. [45], Cerda et al. [46] and De Knijf et al. [47] showed that, for rapid heating of 0.1 % C steel, the high dislocation density and carbon concentration of the initial ferrite was retained upon transformation to austenite. Higher dislocation density increases the work-hardening effect. Although the New-cycle can possibly lead to retention of the favorable high dislocation density and greater strength, none of the cycles showed any significant difference in the work-hardening rate. A significant change in dislocation density was found between AB and heat-treated specimens built in a similar EOS M280 machine at the CRPM by Muiruri et al. [47]. They reported dislocation densities for the AB, SR (650 3 h FC) and annealed (800 2.5 h FC) of 3.82×10^{-15}, 1.02×10^{-15} and 5.73×10^{-14} m^{-2}, respectively [48].

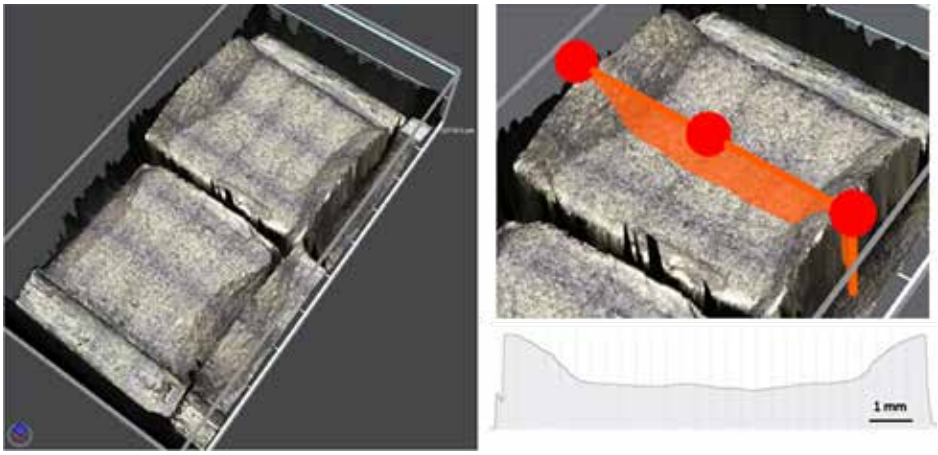

Figure 12: Fracture surfaces of vertical V-notch impact specimen (left) and corresponding depth profile (right).

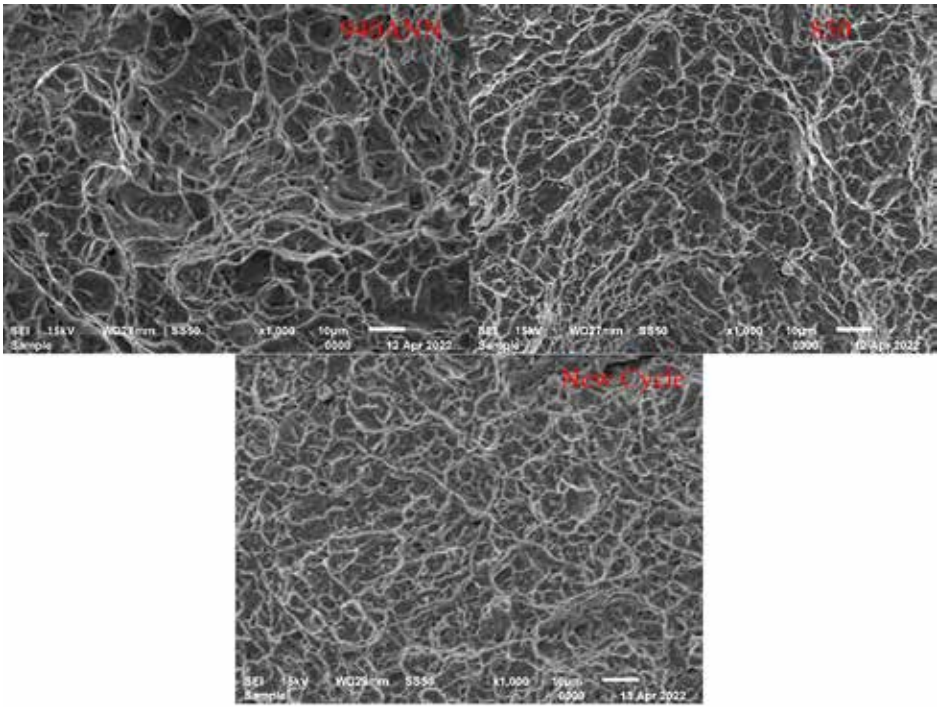

Figure 13: SEM fractographs of vertical tensile specimens heat treated at 940-ANN, 850-ANN, and New-cycle.

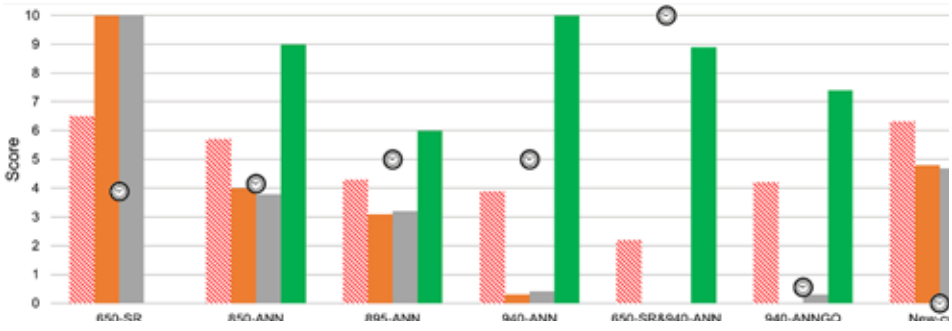

Figure 14: Calculated scores for each cycle.

4.2 Practical considerations: cycle

The New-cycle consisted of slow ramping to 600°C then more rapid heating to 940°C. No hold was present upon reaching 940°C. The initial ramp was slow to allow for stress relief and prevention of deformation. After the component had reached a temperature of 600°C after two hours, the slow ramp had also allowed for temperature uniformity and stress relief, which agrees with the cantilevers having shown no visible deformation and with the findings of Ter Haar and Becker [16], who showed that above 610°C almost all residual stress was relieved within the first five minutes. An additional contribution to this is the relatively small thicknesses of AM parts when compared to industrial parts. After the components had slowly reached temperatures of 600°C and above, the temperature distribution was uniform, and the temperature-dependent yield stress had been lowered so that subsequent rapid heating would not lead

to distortion. The ramp down was controlled and slowed to allow for more time in the temperature range where diffusion can occur (above 750°C) to ensure a more uniform temperature, irrespective of the furnace load. This results in consistency across different-sized builds, with consequent lower induced thermal stress and distortion. Since no air or water cooling is introduced, no descaling or machining is needed to remove oxides. To obtain better statistical reliability of the tensile properties of specimens submitted to the New-cycle, multiple LPBF builds were combined with multiple heat treatment cycles with a total of 15 tensile specimens.

4.3 Practical considerations: time, cost, and performance

Although most of these heat-treatment cycles produced excellent mechanical properties when compared to wrought Ti6Al4V (as found in [2]) and are all above the requirements of ASTM F3001–14, from a practical point of view, reduced cycle time and cost are of major importance. Therefore, each cycle was scored based on a very simple calculation: the maximum value of each property scored 10 points, while the lowest scored zero points, and anything in between was interpolated linearly between the maximum and minimum points. The scores and actual times of the cycles are shown in Figure 13.

In this scoring system, the 650-SR cycle only just beat the New-cycle and scored 0.2 more on average than the New-cycle, which is in second place, with the 850-ANN cycle in third place. Although the 650-SR cycle is in the first place, its low elongation should be noted, which is not clearly represented by this scoring system. Performing only a stress-relieving heat treatment does not optimize the mechanical properties for improved fatigue life performance. From a time-saving point of view, the New-cycle has a considerably lower cycle time of only four hours, with the 940-ANNGQ close on its heels. However, the latter has the disadvantage of creating larger grain structures and considerably lower yield stress and UTS. Therefore, because of the application of the New-cycle, parts for heat treatment can be received and delivered in half a working day, which has significant time- and cost-saving advantages.

5 CONCLUSION

The purpose of this article was to show that an alternative vacuum heat treatment cycle, considering all the technical aspects of AM, can be used to save time and money. The New-cycle offers a significant reduction in time (from 40 to 4 h), making it cost-effective to maximize the advantages of AM by offering parts that need no further descaling or machining. A yield stress of 987 MPa, higher than all other conventional treatments, was obtained while still having an elongation of 16%. This cycle delivered exceptional tensile and impact properties and sufficiently decomposed the as-built martensite into an $\alpha+\beta$ phase while retaining a very fine microstructure conducive to improved fatigue properties. In this case, the saying "less is more" rings true.

CREDIT AUTHORSHIP CONTRIBUTION STATEMENT

Dean Kouprianoff: Conceptualization, Methodology, Writing-Original draft preparation Willie du Preez: Conceptualization, Reviewing and Editing.

DECLARATION OF COMPETING INTEREST

The authors declare that they have no known competing financial interests or personal relationships that could have appeared to influence the work reported in this article.

ACKNOWLEDGEMENTS

The Collaborative Program in Additive Manufacturing (CPAM), (CSIR-NLC-CPAM-21-MOA-CUT-01), funded by the South African Department of Science and Innovation, is acknowledged for financial support. The Centre for Rapid Prototyping and Manufacturing (CRPM) is acknowledged for assistance and financial support.

REFERENCES

[1] T. Wohlers. Wohlers Report 2019. Additive Manufacturing and 3D Printing State of the Industry, Annual Worldwide Progress Report (2019).

[2] M.J. Donachie. Titanium: a technical guide ASM International (2000).

[3] M. Motyka. Martensite formation and decomposition during traditional and AM processing of two-phase titanium alloys–an overview. Metals, 11 (3) (2021), p. 481, 10.3390/met11030481.

[4] ASTM, 2022. Committee F42 on Additive Manufacturing Technologies. (Online) Available from: https://www.astm.org/COMMITTEE/F42.htm (Accessed on 29 March 2022).

[5] B. Blakey-Milner, P. Gradl, G. Snedden, M. Brooks, J. Pitot, E. Lopez, M. Leary, F. Berto, A. du Plessis. Metal additive manufacturing in aerospace: a review. Mater. Des., 209 (2021), Article 110008, 10.1016/j.matdes.2021.110008.

[6] ISO, 2022. Technical committees ISO/TC 261 Additive Manufacturing. (Online) Available from: https://committee.iso.org/home/tc261 (Accessed on 18 June 2022).

[7] B. Vrancken, L. Thijs, J.P. Kruth, J. Van Humbeeck. Heat treatment of Ti6Al4V produced by selective laser melting: microstructure and mechanical properties. J. Alloy. Compd., 541 (2012), pp. 177-185, 10.1016/j.jallcom.2012.07.022.

[8] P. Krakhmalev, G. Fredriksson, I. Yadroitsava, N. Kazantseva, A. du Plessis, I. Yadroitsev. Deformation behavior and microstructure of Ti6Al4V manufactured by SLM. Phys. Procedia, 83 (2016), pp. 778-788, 10.1016/j.phpro.2016.08.080.

[9] J.P. Kruth, M. Badrossamay, E. Yasa, J. Deckers, L. Thijs, J. Van Humbeeck. Part and material properties in selective laser melting of metals 16th International Symposium on Electromachining (ISEM XVI) edition:16, Shanghai, China (2010), pp. 19-23.

[10] I. Yadroitsev, I. Yadroitsava. Evaluation of residual stress in stainless steel 316L and Ti6Al4V samples produced by selective laser melting. Virtual Phys. Prototyp., 10 (2) (2015), pp. 67-76, 10.1080/17452759.2015.1026045.

[11] D. Agius, K.I. Kourousis, C. Wallbrink. A review of the as-built SLM Ti-6Al-4V mechanical properties towards achieving fatigue resistant designs. Metals, 8 (1) (2018), p. 75, 10.3390/met8010075.

[12] ASTM F3001–14, Standard Specification for Additive Manufacturing Titanium-6 Aluminum-4 Vanadium ELI (Extra Low Interstitial) with Powder Bed Fusion, ASTM International, West Conshohocken, PA, 2014, www.astm.org DOI: 10.1520/F3001–14.

[13] T.F. Broderick, A.G. Jackson, H. Jones, F.H. Froes. The effect of cooling conditions on the microstructure of rapidly solidified Ti-6Al-4V Metall. Trans. A, 16 (11) (1985), pp. 1951-1959.

[14] J. Yang, H. Yu, J. Yin, M. Gao, Z. Wang, X. Zeng. Formation and control of martensite in Ti-6Al-4V alloy produced by selective laser melting. Mater. Des., 108 (2016), pp. 308-318, 10.1016/J.MATDES.2016.06.117.

[15] I. Van Zyl, I. Yadroitsava, I. Yadroitsev. Residual stress in Ti6Al4V objects produced by direct metal laser sintering. South Afr. J. Ind. Eng., 27 (4) (2016), pp. 134-141, 10.7166/27-4-1468.

[16] G. Ter Haar, T. Becker. Low temperature stress relief and martensitic decomposition in selective laser melting produced Ti6Al4V. Mat. Des. Process Comm. (2020), 10.1002/mdp2.138.

[17] S. Leuders, M. Thöne, A. Riemer, T. Niendorf, T. Tröster, H.A. Richard, H.J. Maier. On the mechanical behaviour of titanium alloy TiAl6V4 manufactured by selective laser melting: fatigue resistance and crack growth performance. Int. J. Fatigue, 48 (2013), pp. 300-307, 10.1016/j.ijfatigue.2012.11.011.

[18] S. Cao, R. Chu, X. Zhou, K. Yang, Q. Jia, C. Voon, S. Lim, A. Huang, X. Wu. Role of martensite decomposition in tensile properties of selective laser melted

Ti-6Al-4V. J. Alloy. Compd., 744 (2018) (2018), pp. 357-363, 10.1016/j.jallcom.2018.02.111.

[19] S. Cao, Q. Hu, A. Huang, Z. Chen, M. Sun, J. Zhang, C. Fu, Q. Jia, C. Voon, S. Lim, R. Boyer, Y. Yang, X. Wu. Static coarsening behaviour of lamellar microstructure in selective laser melted Ti–6Al–4V. J. Mater. Sci. Technol., 35 (8) (2019), pp. 1578-1586, 10.1016/j.jmst.2019.04.008.

[20] I. Yadroitsev, P. Krakhmalev, I. Yadroitsava. Selective laser melting of Ti6Al4V alloy for biomedical applications: Temperature monitoring and microstructural evolution. J. Alloy. Compd., 583 (2014), pp. 404-409, 10.1016/j.jallcom.2013.08.183.

[21] G. Ter Haar, T. Becker. Selective laser melting produced Ti-6Al-4V: Post-process heat treatments to achieve superior tensile properties. Materials, 11 (1) (2018), 10.3390/ma11010146.

[22] R. Sabban, S. Bahl, K. Chatterjee, S. Suwas. Globularization using heat treatment in additively manufactured Ti-6Al-4V for high strength and toughness. Acta Mater., 162 (2019), pp. 239-254, 10.1016/J.ACTAMAT.2018.09.064.

[23] Z. Zou, M. Simonelli, J. Katrib, G. Dimitrakis, R. Hague. Refinement of the grain structure of additive manufactured titanium alloys via epitaxial recrystallization enabled by rapid heat treatment. Scr. Mater., 180 (2020), pp. 66-70, 10.1016/j.scriptamat.2020.01.027.

[24] A. Baker, P. Collins, J. Williams. New nomenclatures for heat treatments of additively manufactured titanium alloys. JOM, 69 (7) (2017), pp. 1221-1227, 10.1007/s11837-017-2358-y.

[25] ASTM F3301-18a, Standard for Additive Manufacturing – Post Processing Methods – Standard Specification for Thermal Post-Processing Metal Parts Made Via Powder Bed Fusion, ASTM International, West Conshohocken, PA, 2018, www.astm.org DOI: 10.1520/F3301-18A.

[26] EOS, 2022. EOS Titanium Ti64 Grade 23 Material Data Sheet. (Online) Available from: https://www.eos.info/03_system-related-assets/material-related-contents/metal-materials-and-examples/metal-material-datasheet/titan/ti64/material_datasheet_eos_titanium_ti64_grade23_premium_en_web.pdf (Accessed on 24 May 2022).

[27] D. Hollander, M. von Walter, T. Wirtz, R. Sellei, B. Schmidt-Rohlfing, O. Paar, H. Erli. Structural, mechanical and in vitro characterization of individually structured Ti–6Al–4V produced by direct laser forming. Biomaterials, 27 (7) (2006), pp. 955-963, 10.1016/j.biomaterials.2005.07.041.

[28] G. Kasperovich, J. Hausmann. Improvement of fatigue resistance and ductility of TiAl6V4 processed by selective laser melting. J. Mater. Process. Technol., 220 (2015), pp. 202-214, 10.1016/j.jmatprotec.2015.01.025.

[29] G. Longhitano, M. Arenas, A. Conde, M. Larosa, A. Jardini, C. de Carvalho Zavaglia, J. Damborenea. Heat treatments effects on functionalization and corrosion behavior of Ti-6Al-4V ELI alloy made by additive manufacturing. J. Alloy. Compd., 765 (2018), pp. 961-968, 10.1016/j.jallcom.2018.06.319.

[30] S. Semiatin, T. Brown, T. Goff, P. Fagin, R. Turne, J. Murry, D. Barker, J. Miller, F. Zhang. Diffusion coefficients for modeling the heat treatment of Ti-6Al-4V. Met. Mater. Trans. A, 35 (2004), pp. 3015-3018, 10.1007/s11661-004-0250-1.

[31] J.P. Kruth, J. Deckers, E. Yasa, R. Wauthlé. Assessing and comparing influencing factors of residual stresses in selective laser melting using a novel analysis method. Proc. Inst. Mech. Eng., Part B: J. Eng. Manuf., 226 (6) (2012), pp. 980-999, 10.1177/0954405412437085.

[32] Vrancken, B., Wauthle, R., Kruth, J.P., Van Humbeeck, J., 2013. Study of the influence of material properties on residual stress in selective laser melting. 24th International SFF Symposium – An Additive Manufacturing Conference, SFF 2013. p.393–407.

[33] D. Buchbinder, W. Meiners, N. Pirch, K. Wissenbach, J. Schrage. Investigation on reducing distortion by preheating during manufacture of aluminum components using selective laser melting. J. Laser Appl., 26 (1) (2014), 10.2351/1.4828755.

[34] J. Lee, M. Lee, S. Yeon, D. Kang, T. Jun. Influence of heat treatment and loading direction on compressive deformation behaviour of Ti–6Al–4V ELI fabricated by powder bed fusion additive manufacturing. Mater. Sci. Eng.: A (2022), p. 831, 10.1016/j.msea.2021.142258.

[35] Y. Liu, H. Xu, B. Peng, X. Wang, S. Li, Q. Wang, Z. Li, Y. Wang. Effect of heating treatment on the microstructural evolution and dynamic tensile properties of Ti-6Al-4V alloy produced by selective laser melting. J. Manuf. Process., 74 (2022), pp. 244-255, 10.1016/j.jmapro.2021.12.035.

[36] D. Malka-Markovitz, A. Katsman, A. Shirizly, M. Bamberger. Microstructure and mechanical properties of heat treated selective laser melting manufactured Ti-6Al-4V. J. Int. Sci. Publ. Mater. Methods Technol. (Online), 10 (2016), pp. 495-505.

[37] ASM Aerospace Specification Metals Inc. Titanium Ti6Al4V (Grade 5), ELI, Annealed. Available online: https://asm.matweb.com/search/SpecificMaterial.asp?bassnum=MTP643 (accessed on 27 May 2022).

[38] G. Ter Haar, T. Becker. The influence of microstructural texture and prior beta grain recrystallisation on the deformation behaviour of laser powder bed fusion produced Ti–6Al–4V. Mater. Sci. Eng.: A, 814 (2021), Article 141185, 10.1016/j.msea.2021.141185.

[39] T. Voisin, N. Calta, S. Khairallah, J.P. Forien, L. Balogh, R. Cunningham, A. Rollett, Y. Wang. Defects-dictated tensile properties of selective laser melted Ti-6Al-4V. Mater. Des., 158 (2018), pp. 113-126, 10.1016/j.matdes.2018.08.004.

[40] W. Xu, E.W. Lui, A. Pateras, M. Qian, M. Brandt. In situ tailoring microstructure in additively manufactured Ti-6Al-4V for superior mechanical performance. Acta Mater., 125 (2017), pp. 390-400, 10.1016/j.actamat.2016.12.027.

[41] A. Singh, F. Yang, R. Torrens, B. Gabbitas. Heat treatment, impact properties, and fracture behaviour of Ti-6Al-4V alloy produced by powder compact extrusion. Materials, 12 (23) (2019), p. 3824, 10.3390/ma12233824.

[42] L. Monaheng, W. du Preez, C. Polese. Towards qualification in the aviation industry: impact toughness of Ti6Al4V(ELI) specimens produced through laser powder bed fusion followed by two-stage heat treatment. Metals, 11 (11) (2021), p. 1736, 10.3390/met11111736.

[43] P. Manikandan, V.A. Kumar, P.I. Pradeep, R. Vivek, K. Sushant, G. Sudarshan, S.V.S. Narayana Murthy, D. Sivakumar, P. Ramesh Narayanan. On the anisotropy in room-temperature mechanical properties of laser powder bed fusion processed Ti6Al4V-ELI alloy for aerospace applications. J. Mater. Sci., 57 (2022), pp. 9599-9618, 10.1007/s10853-022-07032-y.

[44] A. Muiruri, M. Maringa, W. du Preez. Effects of stress-relieving heat treatment on impact toughness of direct metal laser sintering (DMLS)-produced Ti6Al4V (ELI) parts. JOM, 72 (2020), pp. 1175-1185, 10.1007/s11837-019-03862-5.

[45] M. Yonemura, H. Nishibata, T. Nishiura, N. Ooura, Y. Yoshimoto, K. Fujiwara, K. Kawano, T. Terai, Y. Inubushi, I. Inoue, K. Tono, M. Yabashi. Fine microstructure formation in steel under ultrafast heating. Sci. Rep., 9 (2019), p. 11241, 10.1038/s41598-019-47668-6.

[46] F. Cerda, C. Goulas, I. Sabirov, S. Papaefthymiou, A. Monsalve, R. Petrov. Microstructure, texture and mechanical properties in a low carbon steel after ultrafast heating. Mater. Sci. Eng., 672 (2016), pp. 108-120, 10.1016/j.msea.2016.06.056.

[47] D. De Knijf, A. Puype, C. Föjer, R. Petrov. The influence of ultra-fast annealing prior to quenching and partitioning on the microstructure and mechanical properties. Mater. Sci. Eng., 627 (2015), pp. 182-190, 10.1016/j.msea.2014.12.118.

[48] A. Muiruri, M. Maringa, W. du Preez. Evaluation of dislocation densities in various microstructures of additively manufactured Ti6Al4V (ELI) by the method of X-ray diffraction Materials, 13 (2020), p. 5355, 10.3390/ma13235355.

ABOUT THE AUTHORS

Dean Kouprianoff and Willie du Preez are with the Centre for Rapid Prototyping and Manufacturing, Faculty of Engineering, Built Environment and Information Technology, Central University of Technology, Free State, South Africa.